ELSEVIER

Chemical Engineering Journal 135S (2008) S166–S172

Chemical Engineering Journal

www.elsevier.com/locate/cej

μPIV-Analysis of Taylor flow in micro channels

D. Malsch [a], M. Kielpinski [a], R. Merthan [a], J. Albert [a], G. Mayer [a], J.M. Köhler [c], H. Süße [b], M. Stahl [a], T. Henkel [a,*]

[a] *Institute for Physical High Technology e.V. Jena, Albert-Einstein-Street 9, D-07745 Jena, Germany*
[b] *Digital Image Processing Group, Friedrich-Schiller-University Jena, Ernst-Abbe-Platz 1-4, D-07743 Jena, Germany*
[c] *Department of Physical Chemistry and Microreaction Technology, Technical University Ilmenau, Weimarer Straße 32, D-98693 Ilmenau, Germany*

Abstract

Micro particle imaging velocimetry (μPIV) has been used to characterize two-phase flows in micro channels. Phase internal flow in large segments as well as in small segments has been investigated for the contribution of interface friction to the formation of the internal flow field. According to experimental conditions (flow rate, volume ratio of the phases, channel path geometry, viscosity), the decisive contribution of either liquid/wall or liquid/liquid interface friction to the phase internal flow changes locally. This results in partially alternating internal flow directions between micro droplets and separation medium. For internal flow field evaluation, algorithms of PIV image analysis have been extended for algorithms of droplet recognition, mapping and transformation into a single coordinate system before displacement analysis. Simulations by computational fluid dynamics (CFD) are in good agreement with the measured flow fields.

Keywords: Micro channel; Segmented flow; Micro PIV; Taylor flow

1. Introduction

In microfluidic applications, two-phase flow of immiscible fluids transported in micro channel networks offers promising potentials for high throughput sample processing in chemistry and biotechnology. Creation of diverse and individually addressable sample stacks for serial processing, narrow residence time distributions as well as enhanced mixing capabilities are three immediate benefits. These pay off for example in biochemical analysis, nanoparticle synthesis and kinetic measurements [1–7].

Mixing of reagents is the limiting factor in many chemical processes. Selectivity and conversion rate depend on mixing. Based on these preconditions, efficient mixing approaches have been developed and exist in a wide variety of implementations. In single phase flow, passive micro mixers dependent on lamination or chaotic advection to decrease diffusion lengths have been applied [8–11]. Active micro mixers are based on pressure-driven, dielectrophoretic, electro-kinetic or acoustic stimulation [12–15]. Two-phase flow with fluid segments separated by an immiscible fluid or gas offers fast and efficient mixing while limiting axial dispersion in contrast to other passive micro mixers [16–19]. The complex internal flow field in those segments are induced by the shear force between the two immiscible fluids or by liquid/wall friction.

Micro particle imaging velocimetry (μPIV) becomes a powerful tool for the characterization of internal flow fields in micro channels [20]. With its high spatial resolution it can resolve details of the internal flow fields and provides an approved instrument for qualitative and quantitative flow analyses.

In this work we are presenting the measurements of the internal flow fields of liquid/liquid and liquid/gas two-phase systems in all-glass micro channels. After introducing the employed microfluidic chip devices (Section 2) and the basics of segmented flow (Section 3), Section 4 deals with our self-built μPIV setup. Micro PIV of non-stationary objects requires some extensions to the common algorithms of μPIV. These are discussed. In Section 5, μPIV is applied to the investigation of the contribution of fluid/fluid and fluid/wall friction. Liquid/liquid as well as liquid/gas segmented flow have been analyzed. Dependent on experimental conditions, viscosity of the transported fluids and operation conditions multiple flow regimes of Taylor flow

* Corresponding author. Tel.: +49 3641 206 307.
E-mail address: Thomas.Henkel@ipht-jena.de (T. Henkel).

1385-8947/$ – see front matter © 2007 Elsevier B.V. All rights reserved.
doi:10.1016/j.cej.2007.07.065

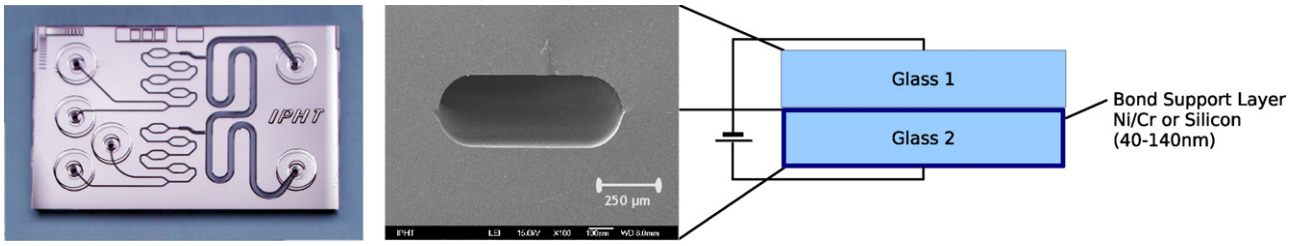

Fig. 1. Left: Microfluidic chip device incorporating segment creation and dosing inlets with pre-mixing of respectively two reagents and a winding main channel for efficient mixing of the dosed reagents. Middle: SEM image of the channel cross-section. Right: schematic of the channel consisting of two half-channels bonded via a bond support layer.

are observed. Gas/liquid two-phase flow is dominated by liquid/wall friction whereas oil/water two-phase flow is dominated by friction at the liquid/liquid interface.

2. Microfluidic chip devices

Our technology of wet etching and anodic bonding of two glass substrates using a bond support layer offers the preparation of microfluidic chip devices with optical transparent micro channels for image based analysis of fluid dynamics and process diagnostics. Moreover, a two-step etching process allows the creation of channels with different etch depths on a single substrate. Two half channel substrates are bonded with a newly developed anodic bonding process. Anodic bonding is mediated by a nickel/chromium [21] or silicon [22] bond support layer. The micro channels may be prepared with channel heights between 100 nm and 260 μm. In our experiments we used micro channels with channel dimensions of 780 μm × 260 μm (Fig. 1).

3. Segmented flow

The concept of segmented flow uses small linearly organized droplets of liquid samples, which are separated by an immiscible separation fluid. These sample stacks are generated, manipulated and controlled in a microfluidic environment as shown in Fig. 2. [21] Microfluidic chip modules and technologies have been developed for generation of diverse sample collections, dosing of reagents to the sample compartments, retrieval of individual compartments and analysis of compartment ingredients and cell counting. Actual research focuses on the development of functional nodes which use interface forces and flow dynamics for development of self-controlling elements for processing of segmented sample streams [23].

Dependent on the channel dimensions droplets may have a volume between a few nanoliters up to several hundred nanoliters. In modular setups micro droplets have a volume of about 60–100 nl and are transported in well controlled plug mode [24]. In most applications segments of water are transported in tetradecane as separation medium. Channel surfaces are treated with octadecyltrichlorosilane in order to generate optimum wettability for mineral oil and minimum wettability for water. For μPIV investigations the water droplets are loaded with yeast cells as tracer particles with a diameter of 4–5 μm.

Phase internal flows are induced by friction at the interfaces (Fig. 3). The liquid/wall as well as the liquid/liquid interface contribute to the flow induction. In large segments the flow is dominated by liquid/wall friction and Taylor flow is observed. In small aqueous micro droplets flanked by large segments of separation medium the contribution of friction at the liquid/liquid interface is increased. This results in an opposite direction of the phase internal flow.

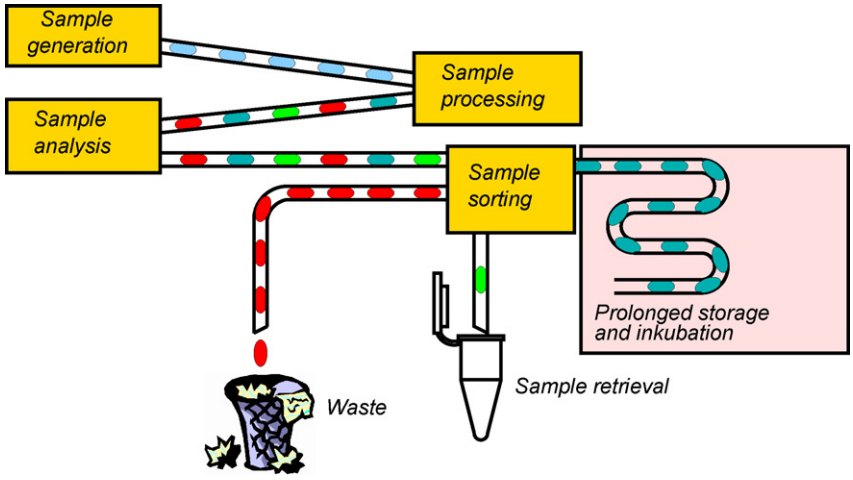

Fig. 2. Segmented flow based high-throughput micro-chemical applications are based on discrete sample streams which are generated, processed, analyzed and controlled using microfluidic chip technology.

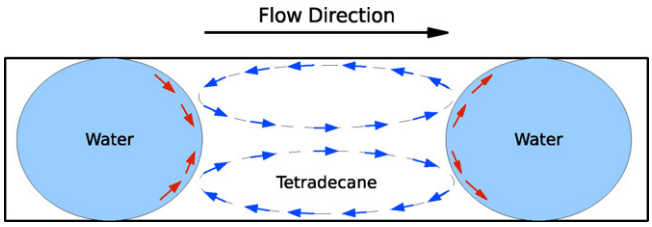

Fig. 3. Contribution of interface friction to the phase internal flow. In large segments it is dominated by liquid/wall friction. Their stable flow field induces a reversed flow direction inside the micro droplets caused by liquid/liquid friction which superposes existing liquid/wall friction.

4. μPIV Setup and algorithms

Tracer particles are visualized via dark field transmission mode illumination with a red high-power LED serving as light source. Image acquisition has been conducted with an Olympus i-SPEED 2 high speed video camera (800 × 600 @ 1,000 fps) and an AVT Marlin video camera (780 × 582 with triggered flashlight double frame exposition). In both cases the cameras have been equipped with 10× microscope lenses with a Numerical Aperture of 0.2 (Fig. 4) ..The depth of focus has been measured with a pinhole to be 100 μm. Each tracer particle in the object plane (1.0 mm × 0.75 mm) is imaged on at least 3–4 pixels in order to get positional sub-pixel resolution by fitting its gray values to a Gauss profile. Image acquisition with the AVT Marlin camera is triggered via the moving fluid/fluid phase boundary of the segments detected by a photo diode. A programmable micro controller allows adjustment of exposure time (flashlight duration) and time between two illuminations (typically 3 ms) (Fig. 5) .

In order to obtain the phase internal flow field rather than the global flow field of the segment translating through the micro channel, segments from both frames have to be transformed into

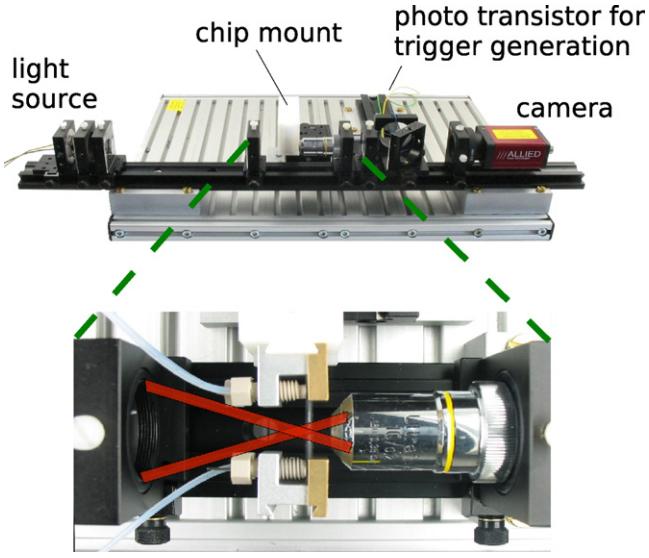

Fig. 4. Optical μPIV setup for double frame exposition in dark field transmission mode. As light source serves a red high power LED, the microscope lens has a 10× magnification and a NA of 0.2. Images are recorded with a Marlin video camera from AVT.

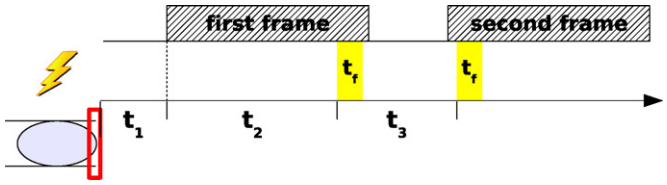

Fig. 5. Time sequence for the programmable flashlight controller for triggered double frame exposition: t_1, time between segment-induced trigger signal and first camera frame; t_2, time offset for first flashlight exposition (t_f flashlight exposition time); t_3, time between first and second flashlight exposition.

the same coordinate system with a segment matching algorithm before PIV analysis. This is done in three steps: First, segments are detected by a gradient based contour detection. Then, based on these contours, a transformation matrix is calculated which comprehends of translation, rotation and optional scaling. Finally, this transformation is applied to the second frame with bilinear interpolation of the gray values for sub-pixel resolution.

PIV analysis is conducted with a self-developed software in cooperation with the Department of Computer Science at Friedrich-Schiller-University Jena. The employed algorithm is based on direct cross correlation extended by the shift detection by restoration method [25]. Sub-pixel resolution is achieved by Gaussian interpolation of the tracer particles.

In contrast to single phase flow with stationary conditions and the possibility for averaging the vector fields or correlation matrices of numerous double-frames [20], two-phase flow does not provide these possibilities. There is only one double exposition for each segment and that means the resulting vector field contains all outliers produced by the correlation algorithm. Thus, an additional step of data validation is required. Our data has been validated with a peak median filter which uses additional information included in the correlation image to reconstruct vectors identified as outliers. Normally, the decision which peak of the correlation image corresponds to the true displacement is to take the one with the highest value. Yet this is problematic in case of peaks with comparable heights where an ancillary peak corresponds to the true displacement rather than the main peak. The peak median algorithm evaluates the main peaks from the neighborhood correlation images and selects the peak in the correlation image whose distance to its neighborhood peaks gets minimal (Fig. 6). Additionally, the algorithm considers a min-

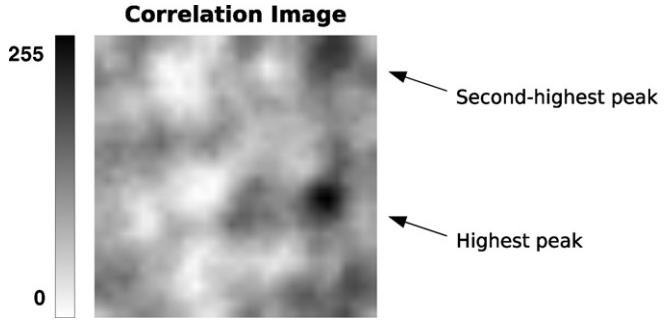

Fig. 6. 32 × 32 pixel correlation image (smoothed) with two peaks corresponding to possible displacement vectors. The peak median algorithm will also consider the second-highest peak if its distance to valid peaks in the neighborhood correlation images is minimal.

imal peak height and implements a parameter accounting for the trade-off between peak height and minimal distance to the neighborhood peaks (equivalent to the smoothness of the vector field). Assuming that the majority of the valid displacement vectors correspond to the main peak and false displacement vectors are statistically distributed, an iterative application of the peak median filter should select valid displacement vectors from the ancillary peaks [26].

Visualization of the measured vector fields and stream line generation with the Runge–Kutta algorithm has been done using the ParaView software [27].

5. Experimental

5.1. Phase internal flow in large segments

For segment internal flow the stable flow fields in the separation medium are the main stimulus for flow field development. Yet PIV measurements of flow fields in the oil phase have been difficult to realize because of the lack of suitable tracer particles. Thus a reverse situation with similar wetting conditions has been chosen where water acts as separation medium between small segments of air. In Fig. 7 phase internal flow is shown for an elongated slug of water flanked by two air bubbles. The flow field shape is non-symmetrical as a result of the air bubble deformation. The internal flow is determined by liquid/wall friction which is in agreement to Günther et al. [28]. Because of the orders of magnitude lower viscosity of air and thus inexistent interface friction, the flow inside these bubbles causes no effect to the flow field in the separation medium. This is in contrast to the oil/water system where there does exist a coupling of both liquid phases over their interface that determines phase internal flow (Fig. 8).

The internal flow field in long segments of water flanked by a transport medium of oil (Fig. 8) is determined by liquid/liquid friction, even though there is a larger liquid/wall

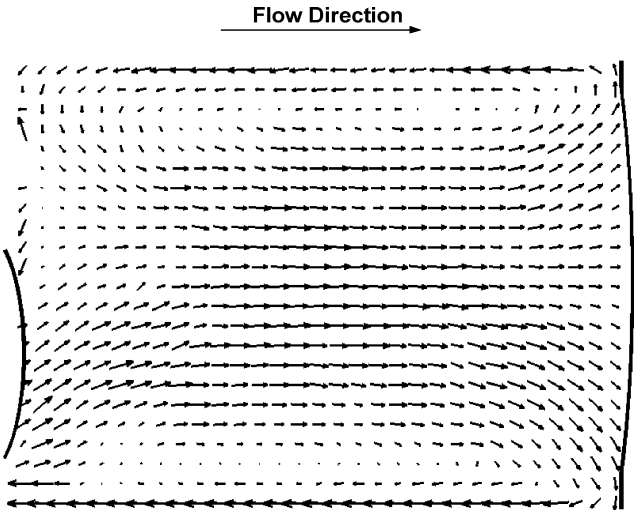

Fig. 7. In long segments of water between two smaller segments of air the internal flow is dominated by liquid/wall friction (transport velocity 5.4 mm/s). Flow inside the air bubbles causes no effect to the flow field in the separation medium because of the orders of magnitude lower viscosity.

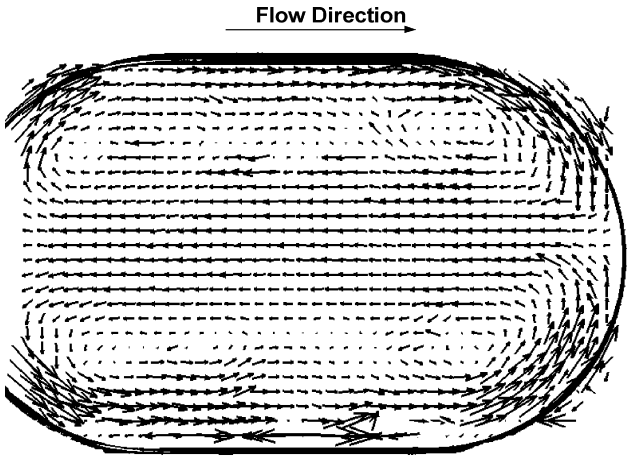

Fig. 8. In long segments of water flanked by long segments of oil, the internal flow is dominated by liquid/liquid friction (transport velocity 2.3 mm/s). A dominating influence of liquid/wall friction like in the water/air system is not recognizable. Complex internal structures can be seen as the existence of six regions with vortices.

than liquid/liquid contact area. A possible explanation is the existence of a thin film of oil wetting the lipophilic channel walls between the water segment resulting in diminished friction. Unlike liquid/wall friction dominated flow found in water segments of air/water flow and in oil segments of oil/water flow, phase internal flow is determined by friction at the liquid/liquid interfaces. There are six regions with vortices, four near the liquid/liquid interfaces and two can be estimated in between. Thus, a total of four regions with liquid/liquid friction dominated flow are found inside the segment. In the central region of the segment the contribution of liquid/wall friction increases, yet liquid/wall friction is not dominating internal flow. This measurement is in agreement with CFD simulations shown below.

5.2. Small segments translating through linear or winding micro channels

For small segments the contribution of the liquid/liquid friction to the phase internal flow is the decisive factor and liquid/wall friction is minimal due to its low interface area. In linear micro channels, the flow field is symmetrical with respect to the channel direction (Fig. 9). Impulse transfer takes place at the four regions with maximum flow at the interface. Each interface region of maximum flow is flanked by a region with circular flow inside the segment. Due to symmetry, mass transfer between the lower and upper half of the segment is restrained which results in a limited mixing efficiency.

A similar behavior is observed for small segments in winding micro channels (Fig. 10). Again, the major contribution to the phase internal flow is induced by the four regions of maximum flow at the liquid/liquid interface. Yet other than for linear channels, flow induction is asymmetric as a result of the channel curvature. This leads to more complex flow fields which results in a faster mass transfer over the whole segment and an improved mixing efficiency.

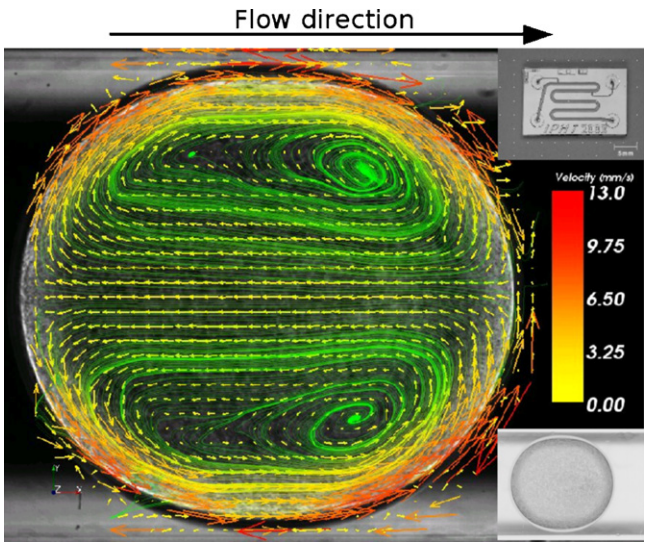

Fig. 9. Reversed symmetrical flow fields are induced by the translation of micro droplets through linear micro channels (transport velocity 7.6 mm/s). Mixing is suppressed. The measured internal flow inside a micro droplet is shown for a micro channel with dimensions of 780 μm × 260 μm. Internal flow is induced at the liquid/liquid interface with four regions of maximum flow.

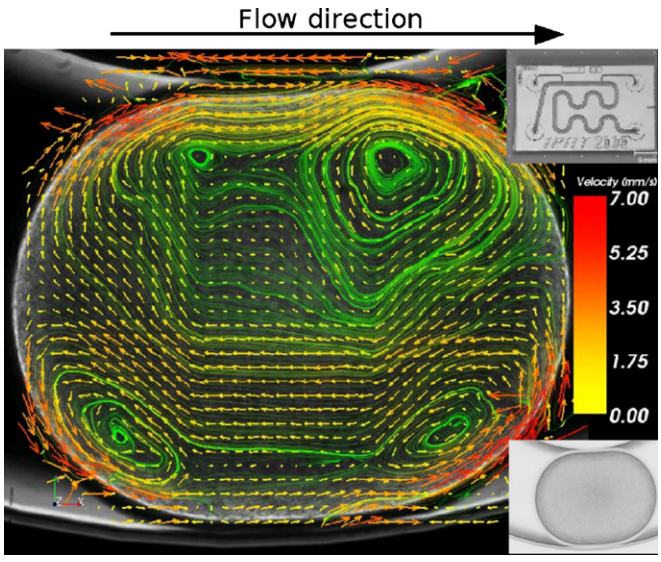

Fig. 10. Translation of droplets through winding channels (transport velocity 7.6 mm/s) induces complex internal flow for efficient mixing. Maximum flow is observed at the liquid/liquid interface which dominates the phase internal flow.

5.3. CFD simulations of phase internal flows

The computational fluid dynamics simulation of phase internal flow in micro channels has been performed with the CFD software Fluent®. Segments of water flanked by separation medium of oil translate through round micro channels with 300 μm in diameter with a transport velocity of 2 mm/s. A contact angle of 160° is adjusted via the boundary layer. Calculations have been conducted with no-slip condition at the channel walls, resulting in an overestimated contribution of liquid/wall friction.

In elongated segments of water flanked by mineral oil, phase internal flow consists of six zones with alternating vortices (Fig. 11). Friction at the liquid/liquid interfaces induces a total of four vortices next to the interface regions. In the middle region of the segment, two more vortices are generated by liquid/wall friction. In small segments liquid/liquid friction determines the internal flow and two main vortices are induced (Fig. 12).

5.4. Flow rate dependency of the phase internal flow in small segments

In small segments the internal flow induction depends on the flow field in the separation medium which is induced by liquid/wall friction. Fig. 13 shows this dependence, which is indicated by the *x*-components of a vertical column of displacement vectors along the segment middle axis, with regard to flow rate. Velocity components smaller than zero indicate flow in transport direction which is found, as already shown, near the liquid/wall phase boundary. This is also true for very small flow rates with hardly any flow induction over the liquid/liquid phase boundary yet also with no measurable flow induction over the

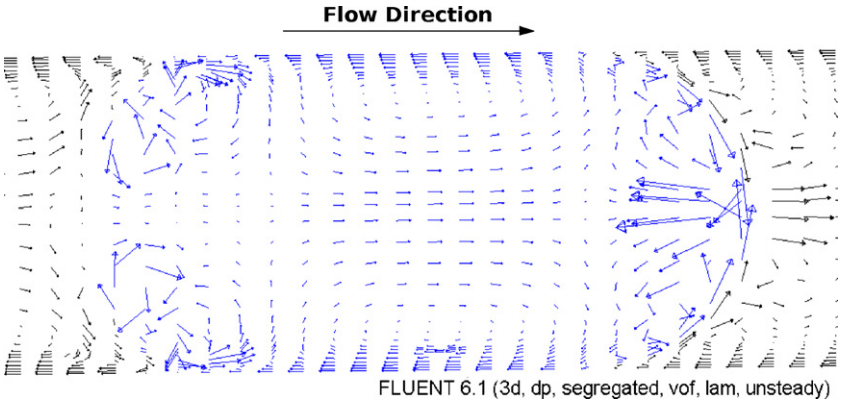

Fig. 11. CFD simulation of the phase internal flow of a long micro droplet translating through a micro channel (transport velocity 2 mm/s). The flow field near the liquid/liquid interface induced by liquid/liquid friction is clearly seen. Inherent to simulation under computational no slip condition, an influence of liquid/wall friction is also represented. Six vortex-regions are apparent, four strong vortices at the liquid/liquid interfaces and two in between, determined by the liquid/wall interface friction.

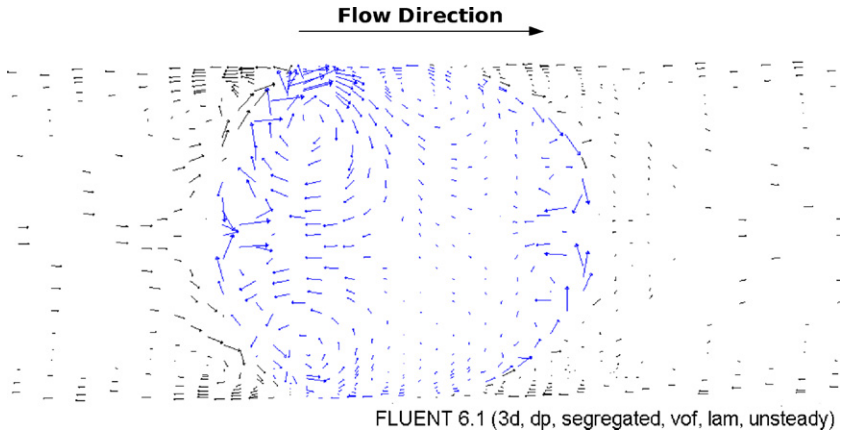

Fig. 12. CFD simulation of the phase internal flow of a micro droplet translating through a micro channel (transport velocity 2 mm/s). The flow field near the liquid/liquid interface induced by liquid/liquid friction is clearly seen. Inherent to simulation under computational no slip condition, an influence of liquid/wall friction is also represented.

liquid/wall phase boundary. The results indicate the absence of any liquid/wall dominated flow in small segments. Higher flow rates result in faster internal flow and stronger flow induction over the liquid/liquid phase boundary. The position of the zero-flow zone in the center of the vortices does not significantly depend on the flow rate.

6. Results and discussion

The concept of segmented flow based on serial high throughput sample processing depends on small sample droplets separated by large segments of a liquid separation medium. In order to ensure maximum reliability for the transport of segmented sample streams, the micro channel wall has to provide optimum wettability for the separation medium and minimum wettability for the sample liquid. This affects the contribution of liquid/wall friction to the internal flow of both fluids. Our results indicate the presence of an ultra thin film of separation fluid between channel wall and sample fluid, which additionally reduces friction between sample liquid and channel wall.

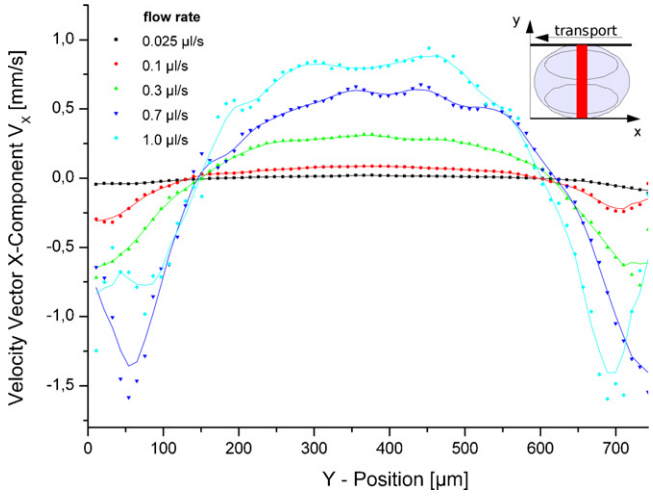

Fig. 13. Flow rate dependency of the internal flow field in small segments translating through linear micro channels. The *x*-component of the displacement vectors along the middle axis of the segment (red stripe in the schematic inset) is plotted against their *y*-position for different flow rates. (For interpretation of the references to colour in this figure legend, the reader is referred to the web version of the article.)

Segment internal flows are induced by friction at the interfaces. The liquid/wall as well as the liquid/liquid interface contribute to the flow induction. In elongated segments of separation medium the flow is dominated by liquid/wall friction and Taylor flow is observed. In small aqueous micro droplets flanked by separation medium the phase internal flow is dominated by friction at the liquid/liquid interface and driven by the more stable, wall friction dominated flow inside the mineral oil which results in an opposite direction of the phase internal flow. A more complicated situation is found in elongated aqueous droplets flanked by mineral oil. At the front and the end of the droplet phase internal flow is determined by friction at the liquid/liquid interfaces. In the central region of the aqueous droplet an additional vortex is induced. These observations are also evident in simulations by CFD where the flow field near the liquid/liquid interface induced by liquid/liquid friction is reversed and an additional vortex between the two outer vortices is found in longish segments.

Fast and efficient mixing of reagents dosed to the sample droplets is strongly dependent on the internal flow fields. Translation of micro droplets in linear channels results in an axial symmetric flow field. This flow obstructs mixing of ingredients inside the droplet. In contrast, translation in curved micro channels results in a superposition of the internal flow with a circular flow field and enables efficient mixing inside the segment. Permanent mass transfer between near-wall and center regions is provided.

These results extend earlier observations during titration experiments [24] or by analysis of dye labeled segment flow [29]. In contrast to these methods, µPIV allows quantitative analysis of the internal flow and provides the fundamentals for development and validation of models for the liquid/liquid two phase flow in micro channels. Thus, they provide the prerequisites for the model based design of highly integrated LabOnChip systems and implementations of the concept of serial organized segmented sample streams [30].

Acknowledgements

This work is part of a joint project with Analytic Jena AG and the Technical University of Ilmenau (FKZ 16SV1998) and has been supported by the Thuringia Ministry of Economy, Technology and Employment (reference number B 309–02007).

The authors thank all co-workers of the project partner and of our institute for their contributions. Special thanks to Dr. Martin Roth and Karin Martin, Leibniz Institute for Natural Product Research and Infection Biology e.V. Hans-Knöll-Institute (HKI) for preparation of the cells applied in this experiments.

References

[1] L.S. Roach, H. Song, R.F. Ismagilov, Anal. Chem. 77 (2005) 785–796.
[2] J.R. Burns, C. Ramshaw, Lab. Chip 1 (2001) 10–15.
[3] D. Huh, Y.C. Tung, H.H. Wei, J.B. Grotberg, S.J. Skerlos, K. Kurabayashi, S. Takayama, Biomed. Microdevices 4 (2002) 141–149.
[4] V. Srinivasan, V.K. Pamula, R.B. Fair, Lab. Chip 4 (2004) 310–315.
[5] I. Shestopalov, J.D. Tice, R.F. Ismagilov, Lab. Chip 4 (2004) 316–321.
[6] H. Song, R.F. Ismagilov, J. Am. Chem. Soc. 125 (2003) 14613–14619.
[7] M.R. Bringer, C.J. Gerdts, H. Song, J.D. Tice, R.F. Ismagilov, Philos. Trans. R. Soc. Lond. Ser. A-Math. Phys. Eng. Sci. 362 (2004) 1087–1104.
[8] A.E. Kamholz, B.H. Weigl, B.A. Finlayson, P. Yager, Anal. Chem. 71 (1999) 5340–5347.
[9] N. Schwesinger, T. Frank, H. Wurmus, J. Micromech. Microeng. 6 (1996) 99–102.
[10] V. Mengeaud, J. Josserand, H.H. Girault, Anal. Chem. 74 (2002) 4279–4286.
[11] S.H. Wong, P. Bryant, M. Ward, C. Wharton, Sens. Actuator B: Chem. 95 (2003) 414–424.
[12] I. Glasgow, N. Aubry, Lab. Chip 3 (2003) 114–120.
[13] J.C. Rife, M.I. Bell, J.S. Horwitz, M.N. Kabler, R.C.Y. Auyeung, W.J. Kim, Sens. Actuator A: Phys. 86 (2000) 135–140.
[14] N.T. Nguyen, Z.G. Wu, J. Micromech. Microeng. 15 (2005) R1–R16.
[15] V. Hessel, H. Lowe, F. Schonfeld, Chem. Eng. Sci. 60 (2005) 2479– 2501.
[16] K. Hosokawa, T. Fujii, I. Endo, Proc IEEE Micr Elect (1999) 388–393.
[17] H. Song, M.R. Bringer, J.D. Tice, C.J. Gerdts, R.F. Ismagilov, Appl. Phys. Lett. 83 (2003) 4664–4666.
[18] S.A. Khan, A. Gunther, M.A. Schmidt, K.F. Jensen, Langmuir 20 (2004) 8604–8611.
[19] B.K.H. Yen, A. Günther, M.A. Schmidt, K.F. Jensen, M.G. Bawendi, Angew. Chem.-Int. Edit. 44 (34) (2005) 5447–5451.
[20] J.G. Santiago, S.T. Wereley, C.D. Meinhart, D.J. Beebe, R.J. Adrian, Exp. Fluids 25 (1998) 316–319.
[21] T. Henkel, T. Bermig, M. Kielpinski, A. Grodrian, J. Metze, J.M. Kohler, Chem. Eng. J. 101 (2004) 439–445 [Ibid. IMRET 7 Lausanne(2003)].
[22] V.G. Kutchoukov, F. Laugere, W. van der Vlist, L. Pakula, Y. Garini, A. Bossche, Sens. Actuator A: Phys. 114 (2004) 521–527.
[23] M. Kielpinski, D. Malsch, G. Mayer, J. Albert, J. Felbel, T. Henkel, IMRET 9 Potsdam (2006).
[24] J.D. Tice, H. Song, A.D. Lyon, R.F. Ismagilov, Langmuir 19 (2003) 9127–9133.
[25] H. Suesse, K. Voss, W. Ortmann, T. Baumbach, Lect. Note. Comput. Sci. 1689 (1999) 33–40.
[26] Marco Stahl, Entwicklung von bildanalytischen Verfahren zur Ermittlung von Strömungsfeldern in bewegten Objekten, Diplomarbeit (2004), Fakultät für Mathematik und Informatik, FSU-Jena, Bewegungsdetektion. in Handbuch ICE, Wolfgang Ortmann, Herbert Süße und andere, Friedrich-Schiller-Universität Jena, Institut für Informatik (1992.2005), http://pandora.inf.uni-jena.de/ice.html.
[27] A.H. Sqillacote, The ParaView Guide, 2006, ISBN 1-930934-17-3.
[28] A. Günther, M. Jhunjhunwala, M. Thalmann, M.A. Schmidt, K.F. Jensen, Langmuir 21 (2005) 1547–1555.
[29] K. Martin, T. Henkel, V. Baier, A. Grodrian, T. Schon, M. Roth, J.M. Kohler, J. Metze, Lab. Chip 3 (2003) 202–207.
[30] N. Gleichmann, D. Malsch, M. Kielpinski, G. Mayer, T. Henkel, Toolkit for computational fluidic simulation and interactive parametrization of segmented flow based fluidic networks, Chem. Eng. J. 135 (2007) S210–S218.